

## COMMUNICATION

# *In operando* observation of temperature-dependent phase evolution in lithium-incorporation olivine cathode



Mengyu Yan<sup>a,1</sup>, Guobin Zhang<sup>a,1</sup>, Qiulong Wei<sup>a</sup>, Xiaocong Tian<sup>a</sup>, Kangning Zhao<sup>a</sup>, Qinyou An<sup>a,\*</sup>, Liang Zhou<sup>a</sup>, Yunlong Zhao<sup>a,b</sup>, Chaojiang Niu<sup>a</sup>, Wenhao Ren<sup>a</sup>, Liang He<sup>a</sup>, Liqiang Mai<sup>a,\*</sup>

<sup>a</sup>State Key Laboratory of Advanced Technology for Materials Synthesis and Processing, Wuhan University of Technology, Wuhan 430070, China

<sup>b</sup>Department of Chemistry and Chemical Biology, Harvard University, Cambridge, MA 02138, USA

Received 19 October 2015; received in revised form 16 January 2016; accepted 28 January 2016  
Available online 19 February 2016

**KEYWORDS**

*In-situ* X-ray diffraction;  
LiFePO<sub>4</sub>;  
Intermediate phases;  
Low temperature

**Abstract**

LiFePO<sub>4</sub> is one of the most outstanding cathodes for the high performance lithium-ion battery, while it is restricted by its unsatisfactory low temperature performance. Here we detect the structural dynamics and reaction routes of LiFePO<sub>4</sub> via operando condition with high rates, well reproducibility over cycles and low temperature in common laboratory X-ray without the synchrotron light source. The intermediate phases between LiFePO<sub>4</sub> and FePO<sub>4</sub>, driven by the overpotential and limited ion transfer rate along the *b* direction at low temperature, are captured. Our results demonstrate that the existence of intermediate can greatly improve the diffusion kinetics of LiFePO<sub>4</sub>. The deep understanding of reaction routes of LiFePO<sub>4</sub> at low temperature will guide the further material optimization design. Besides LiFePO<sub>4</sub>, such high time resolution *in-situ* X-ray diffraction testing method with laboratory source is available to understand the reaction mechanisms of other electrochemical reaction system.

© 2016 Published by Elsevier Ltd.

**Introduction**

Rechargeable lithium-ion batteries (LIBs) show great potential in electrical vehicles, portable electronics, and back-up for wind energy [1–5]. Olivine LiFePO<sub>4</sub> is one of the most promising and safest cathode materials for LIBs [6]. Since

\*Corresponding authors.

E-mail addresses: [anqinyou86@whut.edu.cn](mailto:anqinyou86@whut.edu.cn) (Q. An), [mlq518@whut.edu.cn](mailto:mlq518@whut.edu.cn) (L. Mai).

<sup>1</sup>These authors contributed equally to this work.

the seminal work by Goodenough et al. [7], over 4000 papers have been reported to enhance the performance and understand the lithiation/delithiation mechanisms of  $\text{LiFePO}_4$  [8-12]. At room temperature, the phase transition between  $\text{LiFePO}_4$  and  $\text{FePO}_4$  is considered as a two-phase reaction with a theoretic volume change of 6.8%, due to the limited  $\text{Li}^+$  solubility and miscibility gap in  $\text{LiFePO}_4$  and  $\text{FePO}_4$  [13-15]. Such a large volume change during the phase transition processes traditionally leads to a poor cycling performance in LIBs. However,  $\text{LiFePO}_4$  displays excellent high-rate performance after nanosized [10,16-21]. In numerous studies, the theoretical calculation was used to understand the correlation between the structure and the ionic/electronic transportation properties of  $\text{LiFePO}_4$ , which were further employed to explain the nanosized effect in  $\text{LiFePO}_4$  [22-24]. It is found that the  $\text{Li}^+$  can move quickly in the tunnels along the  $b$  direction. During the cycling, the phase growth is much faster than its nucleation process [25]. Thus, only few particles react, while the majority of particles keep in the stable  $\text{LiFePO}_4$  or  $\text{FePO}_4$  state. This is known as the “Domino-cascade mechanism” [9].

Ceder's group proposed a nonequilibrium solid solution path to understand the high-rate performance of nanosized  $\text{LiFePO}_4$ . During cycling, the high C-rate arouse high overpotential, which changes the  $\text{Li}^+$  reaction route from the thermodynamic control to kinetics control. Instead of undergoing nucleation and two-phase growth processes, the overpotential induces a nonequilibrium  $\text{Li}_x\text{FePO}_4$  ( $0 < x < 1$ ) solid solution path [26]. Recently, Grey's group demonstrated the nonequilibrium facile phase transformation route by high temporal resolution *in-situ* synchrotron X-ray diffraction (XRD) [27]. It provides a new understanding on the high rate capability of electrode materials undergone two phase reactions, during which the intermediate phase forms with a really short life time. The statement above is further confirmed by X-ray absorption near edge structure investigation [28]. As mentioned above, the research on  $\text{LiFePO}_4$  has achieved great progresses on both the electrochemical performance and reaction mechanisms at room temperature. However, further application of  $\text{LiFePO}_4$  is still limited by the unsatisfactory low temperature performance. Therefore, detecting the structural dynamics and reaction routes of  $\text{LiFePO}_4$  at low temperature is meaningful to understand and further optimize the electrochemical performance of  $\text{LiFePO}_4$ .

Herein, we develop an approach to *in situ* probe the reaction in a customized electrochemical cell at high rates and adjustable temperatures for multiple cycles. A two-dimensional XRD ( $\text{XRD}^2$ ) [29], which is available in common laboratory without the synchrotron light source, is employed to probe the electrochemical reaction with high time resolution. In this work, the phase transformation routes of  $\text{LiFePO}_4/\text{FePO}_4$  at different temperatures (253, 273, 293, and 313 K) with various cyclic voltammetry (CV) scan rates (1.4, 2.8, and  $4.2 \text{ mV s}^{-1}$ ) and galvanostatic charge/discharge rates (1, 2, and 5 C) are investigated by *in-situ*  $\text{XRD}^2$  (Co  $K\alpha$  radiation,  $\lambda=1.7902 \text{ \AA}$ , Bruker D8 DISCOVER). We demonstrate the existence of intermediate phases during the lithiation/delithiation processes at low temperature. Moreover, the dynamics determined phase transformation between  $\text{LiFePO}_4/\text{FePO}_4$  at low temperature with/without overpotential is further investigated. At a temperature of

273 K, the ion diffusion rate along the  $b$  direction is greatly limited, which leads to the accumulation of potential, another channel is forced to open, which results in the stronger polarization and the formation of intermediate phases at lower temperature. It is found that, such intermediate phases between  $\text{LiFePO}_4/\text{FePO}_4$  can efficiently inhibit the degradation of ion diffusion coefficient with the decreasing of reaction temperature. Meanwhile, more intermediate phases form during the discharge process than the charge process, due to the high activation energy for the phase transition from  $\text{FePO}_4$  to  $\text{LiFePO}_4$  [30].

## Experimental section

### Material synthesis

The  $\text{LiFePO}_4/\text{C}$  composites were obtained through a sol-gel process followed by sintering. In the preparation, stoichiometric amount of  $\text{LiNO}_3$ ,  $\text{FeCl}_2 \cdot 4\text{H}_2\text{O}$ , and citric acid were dissolved in deionized  $\text{H}_2\text{O}$  to form a homogeneous solution. Ethylene glycol and  $\text{NH}_4\text{H}_2\text{PO}_4$  solution were then added into the above solution. After drying at  $60^\circ\text{C}$  for 24 h, the precursor was heated at  $600^\circ\text{C}$  for 1 h in  $\text{N}_2$  atmosphere to obtain the  $\text{LiFePO}_4/\text{C}$  composites.

### Materials characterization

Materials characterization was conducted by field emission scanning electron microscopy (FESEM, JEOL 7100F) at an acceleration voltage of 10 kV and XRD (Bruker D8 DISCOVER X-ray diffractometer with non-monochromated  $\text{Co-K}\alpha$  X-Ray source). Thermogravimetry/differential scanning calorimetry (TG/DSC) was performed using a Netzsch STA 449C simultaneous thermal analyzer at a heating rate of  $10^\circ\text{C}/\text{min}$  in air. BET surface areas were measured using Tristar II 3020 instrument by nitrogen adsorption of at 77 K. Transmission electron microscopic (TEM) and high-resolution TEM images were recorded with a JSM-2100F STEM/EDS microscope. For *in-situ* XRD testing, an electrochemical cell module with a beryllium window was used, while the slurry was directly cast on the beryllium window.

### Measurement of electrochemical performance

The electrochemical properties were characterized in CR2016 coin cells with lithium foils as the anode. The working electrodes were prepared by mixing the active materials, acetylene black, and carboxyl methyl cellulose at a weight ratio of 6:3:1. The slurry was cast onto Al foil and dried in a vacuum oven at  $150^\circ\text{C}$  for 2 h. The mass loading of active materials was  $1\text{-}2 \text{ mg cm}^{-2}$ . The electrolyte is composed of 1 M  $\text{LiPF}_6$  dissolved in ethylene carbonate/dimethyl carbonate with a volume ratio of 1:1. Galvanostatic discharge/charge cycling behaviors were investigated with a multichannel battery testing system (LAND CT2001A). CV was tested with an electrochemical workstation (CHI 760D). The *in-situ* XRD with variety temperatures are tested by combining the electrochemical workstation (CHI 760D), the two dimensional XRD (Bruker D8 DISCOVER) and a home made temperature controller system (including a ethyl

alcohol based low temperature trap system and a special hot stage instead of the sample stage of XRD).

## Results and discussion

The  $\text{LiFePO}_4/\text{C}$  nanoparticles show an average particle size of  $\sim 43$  nm, which is consistent with the XRD Rietveld refinement data (Figure S1). The  $\text{LiFePO}_4/\text{C}$  exhibits a BET surface area of  $23 \text{ m}^2 \text{ g}^{-1}$  and a carbon content of 8.9 wt% (Figure S2). To explore the electrochemical performance and structural dynamics of  $\text{LiFePO}_4$ , the CV curves were measured at different scan rates and temperatures under operando conditions (Figure 1a-c). It is observed that, the lower the temperature is, the flatter the reduction and oxidation peaks are. With the temperature cooling from 333 K to 253 K, the ion diffusion coefficient decreases almost one order of magnitude. The variation of *in-situ* diffraction patterns during two random cycles at scan rates of 1.4, 2.8 and  $4.2 \text{ mV s}^{-1}$  at 293 K are shown in Figure 1d-i. At a low scan rate of  $1.4 \text{ mV s}^{-1}$ , all the diffraction peaks can be indexed to  $\text{LiFePO}_4$  or  $\text{FePO}_4$  with the space group of *Pnma*, which can agree with the traditional understanding: the  $\text{LiFePO}_4$  peaks disappear, while the  $\text{FePO}_4$  peaks appear and intensify upon charge [31]. There is no obvious continuous positive intensities in the selected individual

diffraction patterns, at the scan rates of 1.4, 2.8 and  $4.2 \text{ mV s}^{-1}$ . (Figure 1i) However, it can be observed between  $41.7^\circ$  and  $42.8^\circ$   $2\theta$  ranges in the image plot of diffraction patterns at  $4.2 \text{ mV s}^{-1}$ , which indicates the possible existence of intermediate phases with lattice parameters between those of  $\text{LiFePO}_4$  and  $\text{FePO}_4$  under thermodynamic equilibrium state [27] (Figure 1f).

The *in-situ* XRD is applied to further detect the structure change of  $\text{LiFePO}_4$  at the scan rates of 1.4, 2.8 and  $4.2 \text{ mV s}^{-1}$  at a relative low temperature of 273 K (Figure 2). The intermediate phases become much more obvious than those at 293 K (Figure 2a-c). Before charging, the XRD pattern of  $\text{LiFePO}_4$  at 273 K is identical to that at 293 K (Figure S3). As charging proceeds, two changes in the XRD patterns can be noticed. First, the (211), (311), and (121) reflections start to broaden asymmetrically. The most obvious asymmetrical broadening is accompanied by the formation of intermediate phases. For example, the (311) reflections of both  $\text{LiFePO}_4$  and  $\text{FePO}_4$  are connected with each other by the positive intensity band (Figure 2d-f). Second, all the selected peaks shift to higher angle after certain cycles at 273 K, which indicates the decrease of unit cell volume. This results in not only reduced capacity, but also sluggish ion diffusion at low temperature. The Randles-Sevcik equation [32,33] (Eq. 1), is used to calculate the ion diffusion coefficients of  $\text{LiFePO}_4$ , where  $I_p$  is the peak current,  $n$  is the

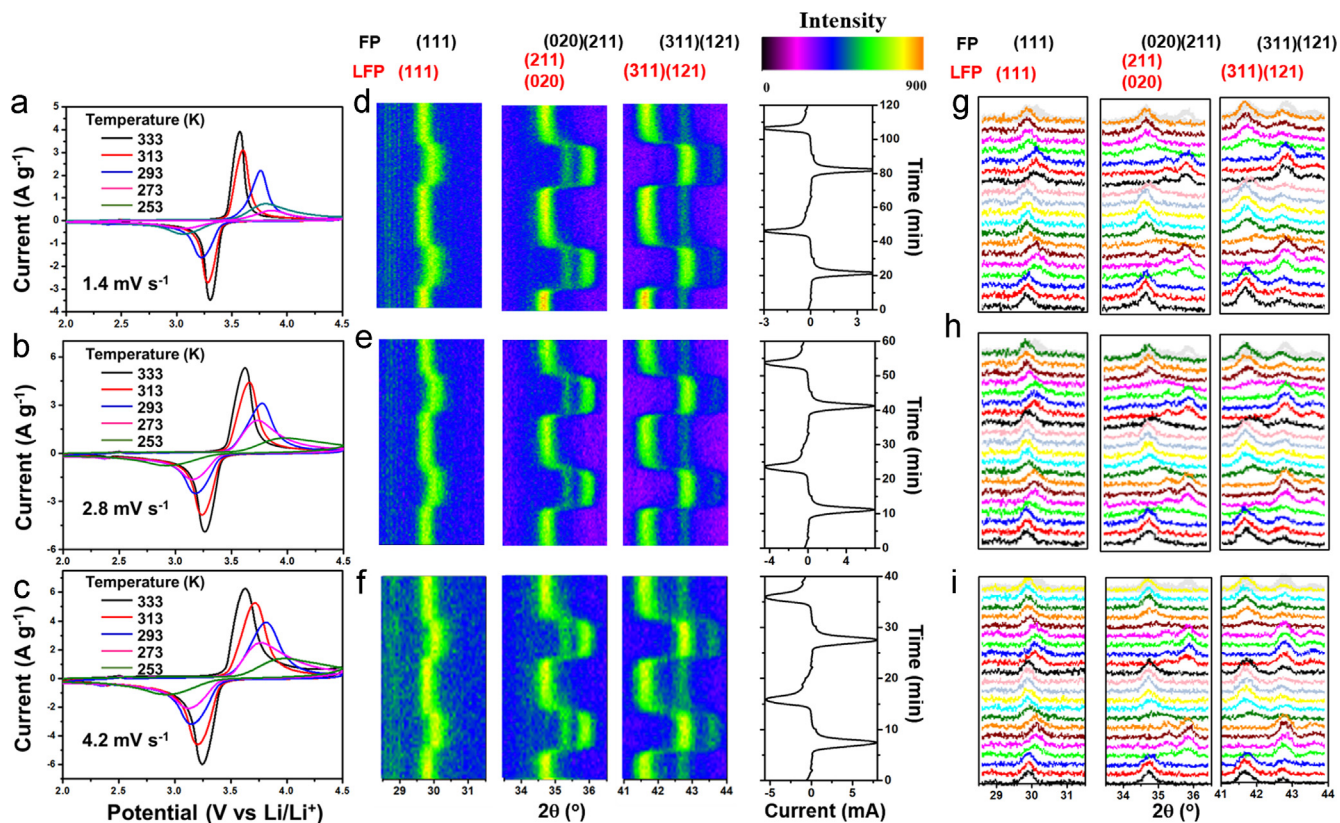


**Figure 1** (a-c) The CV curves of  $\text{LiFePO}_4$  under different scan rates of 1.4, 2.8, and  $4.2 \text{ mV s}^{-1}$  at the temperature ranging from 253-313 K. (d-f) The image plot of diffraction patterns for (111), (211), (020), (311), and (121) reflections during the two CV cycles under different scan rates of 1.4 (d), 2.8 (e), and  $4.2 \text{ mV s}^{-1}$  (f) at a temperature of 293 K. The corresponding current curves are plotted to the right. LFP represent for  $\text{LiFePO}_4$ ; FP represent for  $\text{FePO}_4$ . (g-i) Selected individual diffraction patterns for the two CV cycles at 1.4 (g), 2.8 (h), and  $4.2 \text{ mV s}^{-1}$  (i), corresponding to the results in Figure 1d, e and f, respectively at 293 K.

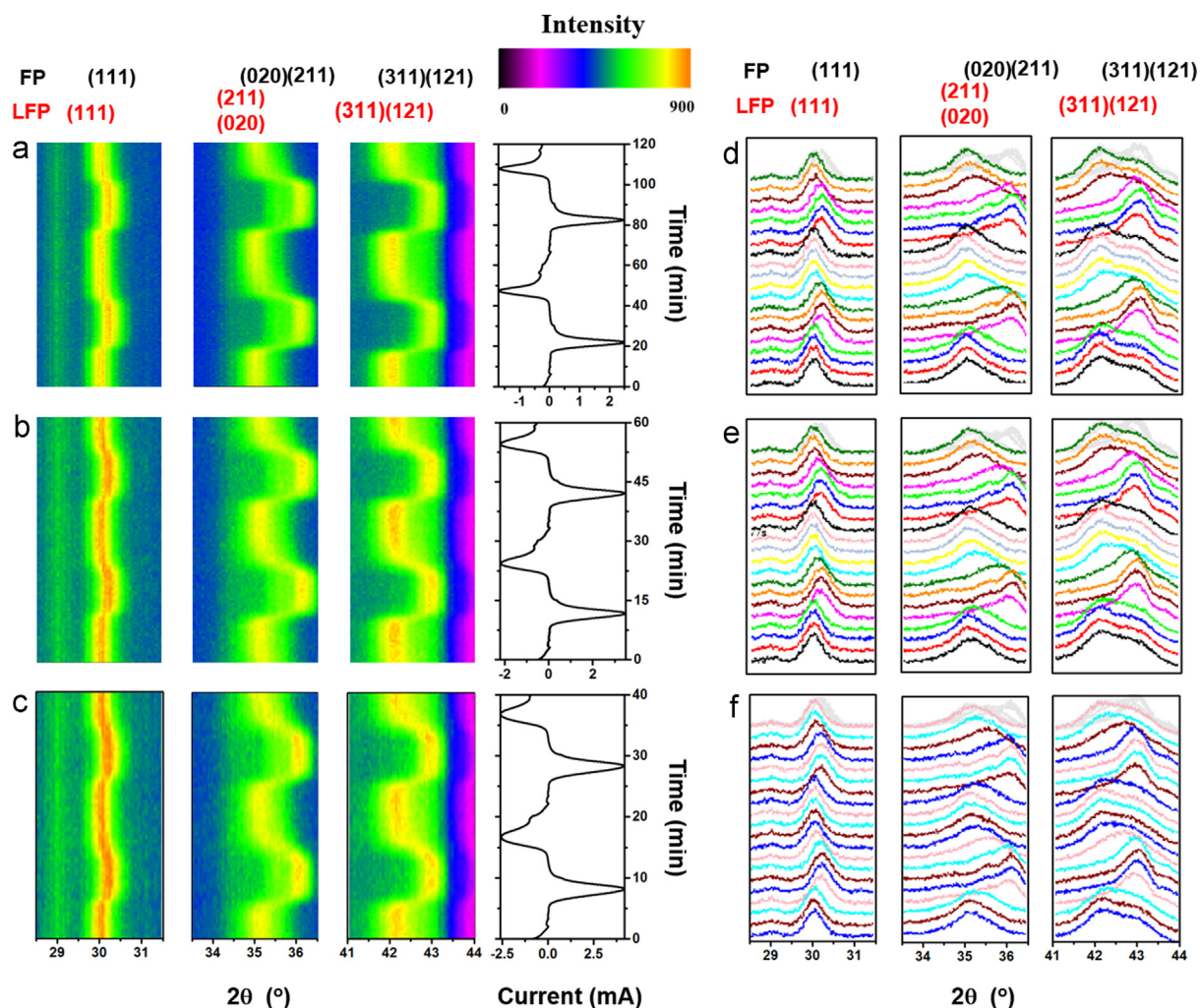


**Figure 2** (a-c) The image plot of diffraction patterns for the (111), (211), (020), (311), and (121) reflections during the two CV cycles under scan rates of 1.4 (a), 2.8 (b), and 4.2 mV s<sup>-1</sup> (c) at a temperature of 273 K. The corresponding current curves are plotted to the right. (d-f) Selected individual diffraction patterns for the two CV cycles at 1.4 (d), 2.8 (e), and 4.2 mV s<sup>-1</sup> (f), corresponding to the results in Figure 1a, b and c, respectively at 273 K.

number of electrons transferred in the redox reaction,  $F$  is the Faraday constant,  $A$  is the active surface area of the electrode,  $C$  is the concentration of Li<sup>+</sup> in the cathode,  $v$  is the scanning rate,  $R$  is the gas constant, and  $T$  is the temperature during measurement.

$$I_p = 0.4463nFAC \left( \frac{nFvD}{RT} \right)^{\frac{1}{2}} \quad (1)$$

From the slope of the fitting line collected from the oxidation peak of the LiFePO<sub>4</sub> (Figure S4), the apparent ion diffusion coefficient  $D$  is calculated to be  $4.65 \times 10^{-13}$ ,  $3.84 \times 10^{-13}$ ,  $2.16 \times 10^{-13}$ ,  $2.14 \times 10^{-13}$  and  $5.50 \times 10^{-14}$  cm<sup>2</sup> s<sup>-1</sup> at the temperature of 333, 313, 293, 273, 253 K, respectively (Table S1). Due to the low coefficient while decreasing the temperature, Li<sup>+</sup> cannot fully insert into the lattice of FePO<sub>4</sub> rapidly, which result in the formation of intermediate phases. The average percentage of diffusion coefficient degradation is calculated at the reaction temperatures of 333, 313, 293, 273 and 253 K which achieves a high

level of 34% per decreasing 20 K. However, the diffusion coefficient  $D$  degrades only 0.93% while decreasing the temperature from 293 to 273 K. (Figure 3a, Table S1) It demonstrates that the formation of intermediate phases can greatly improve the diffusion kinetics of LiFePO<sub>4</sub>. While decreasing the reaction temperature, more intermediate phases lead to less kinetic limitation for LiFePO<sub>4</sub>. Besides, there is more amount of intermediate phases generated at 273 K during the discharge process than those of the charge process, which is due to the high activation energy while FePO<sub>4</sub> transfers to LiFePO<sub>4</sub> (Figure S5) [33]. The intermediate phases are also observed during the charge/discharge processes at 273 K with a rate of 1 and 2 C (Figure S6a and b). However, less intermediate phases form at 253 K, due to the limited reaction activity at extremely low temperature (Figure S6c and d). To further understand the influence of intermediate phases, Total pattern solution (TOPAS) structure refinement package is used to refine the lattice parameter variations during cycling. It is found that, the unit cell parameter  $b$  also changes during cycling, accompanying with the formation of the intermediate phases. At a

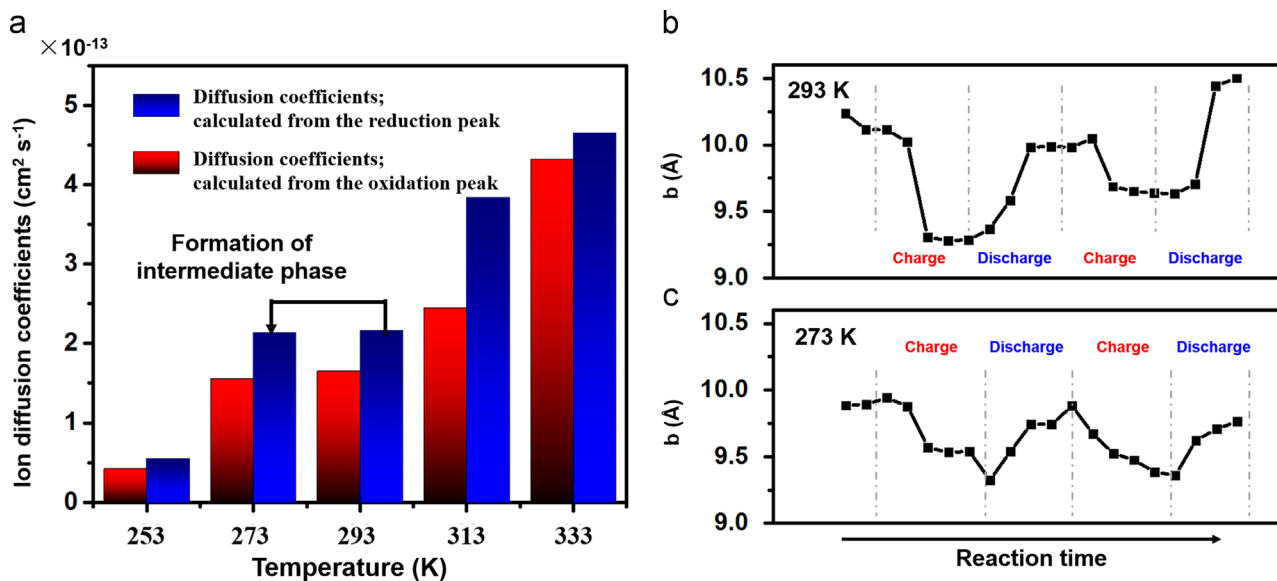


**Figure 3** Temperature determined ion diffusion coefficients and structure evolution. (a) Ion diffusion coefficients of LiFePO<sub>4</sub> at different temperatures. (b,c) The unit cell parameter *b* as a function of reaction time obtained from Rietveld refinement at the temperature of 273 K (b) and 293 K (c) with the scan rate of 1.4 mV s<sup>-1</sup>. All the phases were described in the space group of *Pnma*.

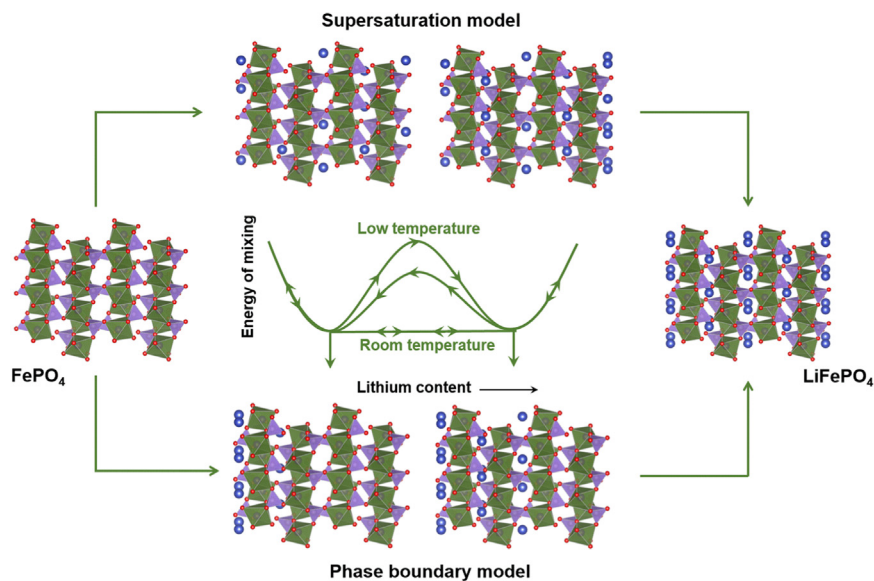


**Figure 4** The schematic pathways of the transformation of FePO<sub>4</sub> to LiFePO<sub>4</sub>. The lower path shows the traditional phase boundary model, which need less energy and undergo an equilibrium thermodynamics processes. The upper path and the upper curve in the center show the high energy pathway via a continuous solid solution called supersaturation model, which shows different mixing energy during the charge and discharge processes.

temperature of 293 K, the LiFePO<sub>4</sub> has a parameter *b* value of ~10.25 Å. With the extraction of Li<sup>+</sup>, the parameter *b* decreases to ~9.25 Å abruptly, which indicates the two phase transition from LiFePO<sub>4</sub> to FePO<sub>4</sub> (Figure 3b). Then, the FePO<sub>4</sub> phase changes back to LiFePO<sub>4</sub> during the anodic process, accompanied by the instantaneous increase of parameter *b*. While cycling at 273 K, the parameter *b* decreases and increases continually with time in the cathodic and anodic processes, respectively, indicating a solid solution reaction between LiFePO<sub>4</sub> and FePO<sub>4</sub> (Figure 3c). It is worth mentioning

that the low temperature also decreases the volume change during cycling from ~7% at 293 K to ~3% at 273 K (analyzed by TOPAS structure refinement). It can be predicted that, the LiFePO<sub>4</sub> forms through intermediate phase process with smaller unit cell volume is more disordered or has a shorter coherence length than that of the stoichiometric LiFePO<sub>4</sub>.

According to the experimental results above, the phase transition model of LiFePO<sub>4</sub> during cycling under room temperature (293 K) and low temperature (273 K) is proposed in Figure 4. At room or higher temperature, the ion

diffusion is fast. During discharge process, the  $\text{FePO}_4$  transfers to  $\text{LiFePO}_4$  almost directly, with an interfacial phase boundary moving with time. Under this process, all of the phases are under thermodynamic equilibrium states. The ion transfer rate is greatly limited with decreasing the temperature to 273 K, which results in the accumulation of overpotential at the interfacial phase boundary of  $\text{LiFePO}_4/\text{FePO}_4$  and the thermodynamic equilibrium state is broken down. Companying with the increase of overpotential, another channel is forced to open, which is predicted by Chiang Group [34]. The phase transition between  $\text{LiFePO}_4$  and  $\text{FePO}_4$  achieves a quasi-equilibrium state with the drive of overpotential, which results in the stronger polarization at lower temperature [35]. Thus,  $\text{FePO}_4$  changes to  $\text{LiFePO}_4$  with a supersaturation model with the inflection of the free energy-composition profile. Such inflected free energy-composition profile leads to the spontaneous disproportionation of phase which also can be understood as intermediate phases or nonequilibrium phases [27]. During the intercalation process, more intermediate phases form resulting from the higher mixing energy. The similar phenomenon is also observed during the charge/discharge processes (Figures S6a and b). Further decreasing the temperature to 253 K, the electroactivity of  $\text{LiFePO}_4$  is reduced due to the sluggish ion intercalation/deintercalation kinetics. Even though, intermediate phases of  $\text{LiFePO}_4$  still can be captured at such a low temperature (Figures S6c and d). It is worth noting that such intermediate phase seems not stable after cycling at ambient temperature. The *ex-situ* HRTEM results show a lattice spacing of 0.303 nm, which matches well with the separation between (0 2 0) planes of  $\text{LiFePO}_4$ . The above phenomenon may be related to the very short life of such metastable state (Figure S7).

## Conclusion

We firstly *in-situ* investigate the structural dynamic and observe the formation of intermediate phases of  $\text{LiFePO}_4$  with high time resolution with laboratory X-ray source. Our experiments allow the electrochemical process to be probed in a wide temperature ranging from 253 to 313 K and the intermediate phases of  $\text{LiFePO}_4$  are captured under the relatively low temperature. The formation mechanism of intermediate phases is further proposed, which is due to the limited ion transfer rate and the accumulate of overpotential at the interfacial phase boundary of  $\text{LiFePO}_4/\text{FePO}_4$ . It is also demonstrated that the existence of intermediate phases inhibit the degradation of ion diffusion coefficient at low environment temperature. Besides  $\text{LiFePO}_4$ , such high-time resolution *in-situ* XRD testing method with laboratory source can also be used to understand the reaction mechanism of other battery electrode materials and related electrochemical reaction system.

## Acknowledgments

M. Yan and G. Zhang contributed equally to this work. This work was supported by the National Basic Research Program of China (2013CB934103, 2012CB933003), the National Natural Science Foundation of China (51521001, 51272197), the International Science & Technology Cooperation Program of

China (2013DFA50840), The Hubei Science Fund for Distinguished Young Scholars (2014CFA035), The National Science Fund for Distinguished Young Scholars (51425204) and the Fundamental Research Funds for the Central Universities (2013-ZD-7, 2014-YB-02). Thanks Professor Q.J. Zhang of Wuhan University of Technology for strong support and stimulating discussions.

## Appendix A. Supplementary material

Supplementary data associated with this article can be found in the online version at <http://dx.doi.org/10.1016/j.nanoen.2016.01.031>.

## References

- [1] J. Liu, *Adv. Funct. Mater.* 23 (2013) 924-928.
- [2] S. Chu, A. Majumdar, *Nature* 488 (2012) 294-303.
- [3] L. Mai, X. Tian, X. Xu, L. Chang, L. Xu, *Chem. Rev.* 114 (2014) 11828-11862.
- [4] M. Armand, J.-M. Tarascon, *Nature* 451 (2008) 652-657.
- [5] B. Dunn, H. Kamath, J.-M. Tarascon, *Science* 344 (2011) 928-935.
- [6] J.J. Wang, X.L. Sun, *Energy Environ. Sci.* 8 (2015) 1110-1138.
- [7] A.K. Padhi, K. Nanjundaswamy, J. Goodenough, *J. Electrochem. Soc.* 114 (1997) 1188-1194.
- [8] F.C. Strobridge, B. Orvananos, M. Croft, H.-C. Yu, R. Robert, H. Liu, Z. Zhong, T. Connolley, M. Drakopoulos, K. Thornton, *Chem. Mater.* 27 (2015) 2374-2386.
- [9] C. Delmas, M. Maccario, L. Croguennec, F. Le Cras, F. Weill, *Nat. Mater.* 7 (2008) 665-671.
- [10] B. Kang, G. Ceder, *Nature* 458 (2009) 190-193.
- [11] N. Ohmer, B. Fenk, D. Samuelis, C.-C. Chen, J. Maier, M. Weigand, E. Goering, G. Schütz, *Nat. Commun.* 6 (2015) 6045.
- [12] X. Zhang, T.W. Verhallen, F. Labohm, M. Wagemaker, *Adv. Energy Mater.* 5 (2015) 1500498.
- [13] C. Ramana, A. Mauger, F. Gendron, C. Julien, K. Zaghib, *J. Power Sources* 187 (2009) 555-564.
- [14] Y. Zhu, J.W. Wang, Y. Liu, X. Liu, A. Kushima, Y. Liu, Y. Xu, S.X. Mao, J. Li, C. Wang, *Adv. Mater.* 25 (2013) 5461-5466.
- [15] L. Laffont, C. Delacourt, P. Gibot, M.Y. Wu, P. Kooyman, C. Masquelier, J.M. Tarascon, *Chem. Mater.* 18 (2006) 5520-5529.
- [16] C. Zhu, Y. Yu, L. Gu, K. Weichert, J. Maier, *Angew. Chem. -Int. Ed.* 50 (2011) 6278-6282.
- [17] C.M. Doherty, R.A. Caruso, B.M. Smarsly, P. Adelhelm, C.J. Drummond, *Chem. Mater.* 21 (2009) 5300-5306.
- [18] Y. Wang, Y. Wang, E. Hosono, K. Wang, H. Zhou, *Angew. Chem. -Int. Ed.* 47 (2008) 7461-7465.
- [19] C.R. Sides, F. Croce, V.Y. Young, C.R. Martin, B. Scrosati, *Electrochem. Solid State* 8 (2005) A484-A487.
- [20] C. Nan, J. Lu, L. Li, L. Li, Q. Peng, Y. Li, *Nano Res.* 6 (2013) 469-477.
- [21] L.H. Hu, F.Y. Wu, C.-T. Lin, A.N. Khlobystov, L.-J. Li, *Nat. Commun.* 4 (2013) 1687.
- [22] D. Morgan, A. Van der Ven, G. Ceder, *Electrochem. Solid ST.* 7 (2004) A30-A32.
- [23] T. Maxisch, F. Zhou, G. Ceder, *Phys. Rev. B* 73 (2006) 104301.
- [24] J. Yang, J.S. Tse, *J. Phys. Chem. A* 115 (2011) 13045-13049.
- [25] M. Wagemaker, D.P. Singh, W.J. Borghols, U. Lafont, L. Haverkate, V.K. Peterson, F.M. Mulder, *J. Am. Chem. Soc.* 133 (2011) 10222-10228.
- [26] R. Malik, F. Zhou, G. Ceder, *Nat. Mater.* 10 (2011) 587-590.

- [27] H. Liu, F.C. Strobridge, O.J. Borkiewicz, K.M. Wiaderek, K.W. Chapman, P.J. Chupas, C.P. Grey, *Science* 344 (2014) 1252817.
- [28] S. Pongha, B. Seekoan, W. Limphirat, P. Kidkhunthod, S. Srilomsak, Y.M. Chiang, N. Meethong, *Adv. Energy Mater.* 5 (2015) 1500663.
- [29] B. B. He, *Two-dimensional X-ray diffraction*, Hoboken, New Jersey, 2011.
- [30] Y. Orikasa, T. Maeda, Y. Koyama, T. Minato, H. Murayama, K. Fukuda, H. Tanida, H. Arai, E. Matsubara, Y. Uchimoto, *J. Electrochem. Soc.* 160 (2013) A3061-A3065.
- [31] H.C. Shin, K.Y. Chung, W.S. Min, D.J. Byun, H. Jang, B.W. Cho, *Electrochem. Commun.* 10 (2008) 536-540.
- [32] D. A. Skoog, D. M. West, *Principles of instrumental analysis*, Delhi, India, 1980.
- [33] P. Zanello, *Inorganic electrochemistry: theory, practice and applications*, Padstow, Cornwall, 2003.
- [34] M. Tang, H.Y. Huang, N. Meethong, Y.H. Kao, W.C. Carter, Y.M. Chiang, *Chem. Mater.* 21 (2009) 1557.
- [35] Y. Kao, M. Tang, N. Meethong, J. Bai, W. Carter, Y. Chiang, *Chem. Mater.* 22 (2011) 21.



**Mengyu Yan** received his B.S. degree in Material Chemistry from China University of Geosciences in 2012 and he is currently working toward the Ph.D degree in Material Science at Wuhan University of Technology. His current research interests include nanoenergy materials and devices.



**Guobin Zhang** received his B.S. degree in Inorganic Non-metallic Materials Engineering from Inner Mongolia University of Science & Technology in 2014 and he is currently working toward the Master. degree. His current research interests include nanomaterials for Li-ions batteries, supercapacitors, sodium batteries and in-situ characterization.



**Qiulong Wei** received his B.S. degree in Department of Materials Science and Engineering from Wuhan University of Technology in 2011. He has joined State Key Laboratory of Advanced Technology for Materials Synthesis and Processing for four years. He is currently working toward the Ph.D. degree. His current research involves the design and synthesis of nanomaterials for achieving both high energy density and

power density electrochemical energy storage device, including the lithium-ion battery, sodium ion battery and the hybrid capacitor.



**Xiaocong Tian** received his first B.S. degree in Materials Physics from Wuhan University of Technology in 2011 and the second B.S. degree in English from Huazhong University of Science & Technology in the same year. He is currently working toward the Ph.D. degree and his current research focuses on the energy storage materials and devices.



**Kangning Zhao** received his B.S. degree in Department of Materials Science of Engineering from Wuhan University of Technology in 2012. He has joined WUT-Harvard Joint Nano Key Laboratory for two years. He is currently working toward the Ph.D. degree. His current research involves the nanomaterials achieving high energy density and power density for lithium ion battery and sodium ion battery.



**Qinyou An** received his Ph.D degree in Material Science at Wuhan University of Technology. His current research interests include nanoenergy materials and devices. He is now a full associate professor at Wuhan University of Technology.



**Dr. Liang Zhou** received his Ph.D (2011) degrees from Department of Chemistry, Fudan University. After graduation, he worked as a postdoctoral research fellow at Nanyang Technological University for 1 year and The University of Queensland for 3 years. He is now a full professor at Wuhan University of Technology and an honorary associate professor at the Australian Institute for Bioengineering and Nanotechnology, The University of Queensland.

His research interests include functional nanomaterials for electrochemical energy storage. Up to now, he has published over 50 papers with a total ISI citation of > 2000 and an h-index of 22.



**Yunlong Zhao** received his B.S. degree in Material Science from the Wuhan University of Technology in 2012 and he is currently working toward the Ph.D degree. His current research interests include nanomaterials for Li-ions batteries, supercapacitors, Li-sulfur batteries and Li-air batteries.



**Chaojiang Niu** received his M.S. degree in Material Chemistry from Wuhan University of Technology in 2009. He is currently working toward the Ph.D. degree and his current research focuses on the energy storage materials and devices.



**Wenhao Ren** received his B.S. degree in material science from Wuhan University of Science and Technology in China in 2012, and He is currently working toward the Ph. D. degree. His current research involves nanoenergy materials and devices.



**Liang He** is an assistant professor of the State Key Laboratory of Advanced Technology for Materials Synthesis and Processing at Wuhan University of Technology. He received his Ph.D. from Tohoku University (Japan) in 2013. His current research interests include the microfabrication and characterization of micro/nano structures and devices for use in MEMS (Micro Electro Mechanical Systems).



**Liqiang Mai** is Chair Professor of Materials Science and Engineering at Wuhan University of Technology (WUT) and Executive Dean of International School of Materials Science and Engineering at WUT. He received his Ph.D. from WUT in 2004. He carried out his postdoctoral research in the laboratory of Prof. Zhonglin Wang at Georgia Institute of Technology in 2006-2007 and worked as advanced research scholar in the laboratory of Prof. Charles M. Lieber at Harvard University in 2008-2011. His current research interests focus on nanowire materials and devices for energy storage. He received the National Natural Science Fund for Distinguished Young Scholars, the First Prize for Hubei Natural Science Award and so forth.